

# Electric-field induced tuning of electronic correlation in weakly confining quantum dots

Huiying Huang,<sup>1,\*</sup> Diana Csontosová,<sup>2,3</sup> Santanu Manna,<sup>1</sup> Yongheng Huo,<sup>4</sup> Rinaldo Trotta,<sup>5</sup> Armando Rastelli,<sup>1</sup> and Petr Klenovsky<sup>2,3,†</sup>

<sup>1</sup>*Institute of Semiconductor and Solid State Physics,  
Johannes Kepler University Linz, Altenbergerstraße 69, A-4040 Linz, Austria*

<sup>2</sup>*Department of Condensed Matter Physics, Faculty of Science,  
Masaryk University, Kotlářská 267/2, 61137 Brno, Czech Republic*

<sup>3</sup>*Czech Metrology Institute, Okružní 31, 63800 Brno, Czech Republic*

<sup>4</sup>*Hefei National Laboratory for Physical Sciences at Microscale,  
and department of Engineering and Applied Physics,*

*University of Science and Technology of China, Hefei, 230026, Anhui, China*

<sup>5</sup>*Department of Physics, Sapienza University of Rome, Piazzale A. Moro 5, 00185 Rome, Italy*

(Dated: June 18, 2022)

We conduct a combined experimental and theoretical study of the quantum confined Stark effect in GaAs/AlGaAs quantum dots obtained with the local droplet etching method. In the experiment, we probe the permanent electric dipole and polarizability of neutral and positively charged excitons weakly confined in GaAs quantum dots. We interpret those results with the help of calculations based on the full-configuration-interaction method which show excellent quantitative agreement with the micro-photoluminescence ( $\mu$ -PL) measurements and allow us to elucidate the role of Coulomb interactions among the confined particles and – even more importantly – of electronic correlation effects on the Stark shifts. Moreover, we show how the electric field alters properties such as built-in dipole, binding energy, and heavy-light hole mixing of multiparticle complexes in weakly confining systems, underlining the deficiencies of commonly used models for the quantum confined Stark effect.

Semiconductor quantum dots (QDs) are one of the most promising quantum light source in quantum technology, as they combine excellent optical properties with the compatibility to semiconductor processing and the potential for scalability. [1–9] Meanwhile, they provide also a platform for photon-to-spin conversion [10, 11], building up bridges between photonic and spin qubits [12–14]. In the process of spin initialization and manipulation [15], the applied electric field ( $F_d$ ) among others modifies the energy and spatial distribution of the confined single-particle (SP) states via the so-called quantum confined Stark effect (QCSE), leading to deep changes in the electronic and optical properties of QDs [16–19]. Therefore, for the possible usage in quantum networks, a fundamental understanding of the effects of  $F_d$  in that kind of quasi-zero dimensional structures is highly desirable.

Here we choose GaAs/AlGaAs QDs fabricated by the local droplet etching (LDE) method [20–25] via molecular beam epitaxy (MBE) as our investigation subject. Superior than other QDs formed by conventional strain or droplet epitaxy, LDE GaAs QD has negligible strain and minimized intermixing of core and barrier material [20–22, 26], thus, are particularly clean and favorable platform both for fundamental investigations and application of QCSE. Meanwhile, because of their state-of-the-art photon indistinguishabilities [27] and near-unity entanglement fidelities of 0.978(5) [28], devices based on LDE GaAs QDs have recently succeeded in the demonstration of entanglement swapping [29, 30] and the quantum key

distribution. [31, 32]

To the best of our knowledge, only a few works have been dealing with the physics of GaAs QDs in externally applied electric fields. [15, 33–38] As an example, in Refs. [37, 38]  $F_d$ 's applied perpendicular to the growth plane were used to modify the Fine structure splitting (FSS) of neutral excitons ( $X^0$ ) confined in natural GaAs QDs (thickness or alloy fluctuations in thin quantum wells, with poorly defined density, shape, and optical properties). Besides that, simplified simulation models based on the SP assumption were built up to explain the effect of charge noise caused by trapping/detrapping occurring at random places in the host material around QD, [39] but neither fully explain the behavior of the charge carriers, nor take into account correlation effects [33] completely. On the contrary, we note that correlation is of particular importance in the GaAs/AlGaAs QD system because of the generally large size of the studied dots. [40–42] For example, excluding the correlation effects, the binding energy ( $E_b$ ) of positively charged exciton ( $X^+$ ) with respect to  $X^0$  shall be rather small and attain negative (anti-binding state) rather than positive (binding state) values, [43] contrasting with the experimental observations. [44–46] Positive  $E_b$  have been theoretically calculated for GaAs QDs obtained by “hierarchical self-assembly”, [41] yet still not quantitatively agreeing with experiment. In addition, detailed studies of the electric field effects on the Coulomb interactions between electrons ( $e^-$ ) and holes ( $h^+$ ) in GaAs QDs are still lacking.

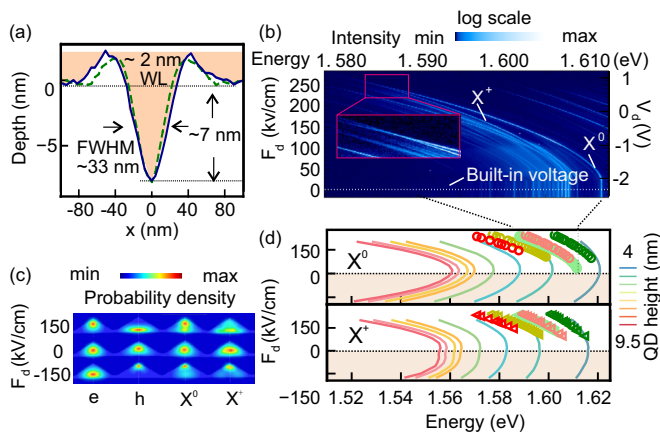


FIG. 1. (a) AFM depth profile of a typical Al-droplet-etched NH. The solid and dashed lines were taken along [110] and [1-10] crystal direction of (Al)GaAs. The orange color indicates the GaAs filling. (b) color-coded PL spectra of QD1 embedded in a p-i-n diode as a function of  $F_d$  and corresponding applied voltage  $V_d$ . Inset: zoomed-in and intensity-enhanced part of the spectra, where we observe the crossing of  $X^0$  and  $X^+$ . (c) Cross-sectional view of the probability densities of  $e^-$ ,  $h^+$ ,  $X^0$ , and  $X^+$  for several values of  $F_d$ . (d) Measured and calculated Stark shifts of  $X^0$  and  $X^+$  for five QDs (symbols) and simulation (curves) for  $X^0$  (top) and  $X^+$  (bottom), respectively. The simulated cone-shaped dots have a fixed base diameter of 40 nm and height varying from 4 nm to 9.5 nm. Note that the QD1 data (light green) correspond to those in panel (b), while data of QD2-QD5 were taken from a series of polarization resolved measurements for  $F_d$  in the range of 100 – 250 kV/cm.

In this work, we conduct a combined experimental and theoretical study of the QCSE in individual GaAs QDs. Our experiments, based on micro-photoluminescence ( $\mu$ -PL) spectroscopy, offer direct information on the permanent electric dipole moment ( $\mathbf{p}$ ) and polarizability ( $\beta$ ) of relevant energy states in GaAs QDs, which sensitively depend on carrier interactions in those nanostructures. Furthermore, we perform calculations of the aforementioned complexes using the configuration-interaction (CI) method [47–50] with SP basis states obtained using the eight-band  $\mathbf{k}\cdot\mathbf{p}$  method computed with the inclusion of the full elastic strain tensor and piezoelectricity (up to second order [51–53]) by Nextnano [54] software package.

We start by measuring the Stark shifts of  $X^0$  and  $X^+$  states of GaAs QDs by  $\mu$ -PL spectroscopy. The shape of the QD is defined by the Al-droplet-etched nanohole (NH) (see Fig. 1 (a)), with depth of  $\sim 7$  nm, full width at half maximum depth of  $\sim 33$  nm) and  $\sim 1 - 2$  nm thick “wetting layer” (WL) above the NHs formed by the GaAs filling. [25, 55] In order to apply  $F_d$  along the growth direction, the QDs were embedded in the intrinsic region of a p-i-n diode structure. [56]

Figure 1 (b) shows typical PL spectra obtained from a QD (marked as QD1) as a function of  $F_d$ . Near  $F_d = 0$ ,

an isolated  $X^0$  transition is found at 1.611407(2) eV, accompanied by multiexciton states at lower energies (1.60843 – 1.60381 eV). This configuration qualitatively agrees with other reports on GaAs QDs grown by LDE, [15, 43, 46] droplet epitaxy, [57] and hierarchical self-assembly, [40, 41] and is different from that observed in In(Ga)As QDs, for which  $X^+$  usually attains higher energy compared to  $X^0$ . [18, 58, 59] Energy shifts for  $F_d \lesssim 30$  kV/cm are not observed in our experiments because of the current injection in the diode. Investigations on the electroluminescence (EL) of this type of device have been reported previously in Ref. 60. For  $F_d \gtrsim 240$  kV/cm the  $\mu$ -PL signal is faint and cannot be tracked because of the field ionization of excitons. [59] Overall, the emission energy is red-shifted by almost 24 meV upon increasing  $F_d$ . We extract the energy of  $X^0$  and  $X^+$  by performing Gaussian fitting of  $\mu$ -PL spectra and for the corresponding  $F_d$  of five QDs and plot those in Fig. 1 (d).

In the simulation we have modeled the NH as a cone with the basal diameter of 40 nm, height of 4 – 9.5 nm and WL thickness of 2 nm. Note, that in order to show that our theory results are more general, we also compute lens-shape dots with same basal diameter and heights as for the reference cone-shaped dots. The simulated Stark shifts of the QDs are plotted together with the experimental data from five dots in the Fig. 1 (d). Calculation results are also shown for  $F_d < 0$ , which is however not experimentally accessible with the present diode structure. Interestingly, the parabolic shifts are not symmetric around  $F_d = 0$ , as already predicted in Ref. 33. Concomitantly, the maximum of the emission energy appears at  $F_d > 0$ . Both effects are the result of the asymmetric shape of QDs along the  $F_d$  direction, i.e.,  $z$ -axis combined with the different behaviors of  $e^-$  and  $h^+$  as their wavefunctions move along  $z$ -axis, thus, experiencing different lateral confinements. On the other hand, the maximum of emission energy at non-zero  $F_d$  can be interpreted with the existence of a permanent electric dipole, which we will discuss in the following.

The shifts of the  $X^0$  and  $X^+$  induced by  $F_d$  are commonly described by the quadratic equation

$$E(F_d) = E_0 + p_z F_d + \beta F_d^2, \quad (1)$$

where  $E_0$  is the emission energy for  $F_d = 0$ , and  $p_z$  and  $\beta$  can be intuitively interpreted as the permanent electric dipole moment and polarizability of the corresponding complexes, respectively. [19, 59, 61, 62] The quantity  $p_z/e$  can be seen as the distance between  $e^-$  and  $h^+$  probability densities along the  $z$ -axis, see also Fig. 1 (c).

Figure 2 (a) summarizes the fitted values of  $p_z/e$  for  $X^0$  and  $X^+$  for five QDs. [64] The negative  $p_z/e$  values are close to the experimental data reported in Ref. 65 ( $p_z/e = -0.39$  and  $-0.31$  nm for QD1 and QD2).

In order to deduce  $p_z/e$  also from our theory data, we first tested the same method as for experiment, i.e., fit-

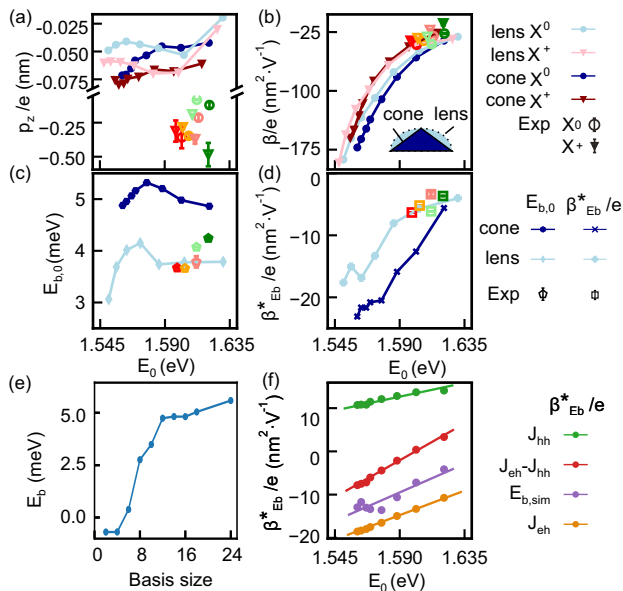


FIG. 2. (a) Permanent electric dipole moments plotted as a function of the zero field energy  $E_0$  of the corresponding complex  $X^0$  or  $X^+$ . (b) Polarizability ( $\beta$ ) as a function of  $E_0$ . Insets: Sketch of the cone- and lens-shaped dots used in the simulation, respectively. Note that the height and diameter of the dot are not shown in the same scale. For (a) and (b): the experimental data (discrete symbols) were extracted from the Stark shift of five measured QDs in Fig. 1 (d) by fitting using Eq. (1) and presented in the corresponding color. (c)  $E_{b,0}$  and (d)  $\beta_{E_b}^*/e$  as the function of  $E_0$  fitted by Eq. (3). The theory values of  $E_{b,0}$  in (c) were obtained directly from CI calculations, i.e., without fitting, while  $\beta_{E_b}^*/e$  in (d) were obtained by fitting theory values using Eq. (3). [63] (e) Dependence of  $E_b$  on the number of SP  $e^-$  and SP  $h^+$  states used in CI basis calculated for QD with height  $h = 9.5$  nm. Note that we used symmetric basis, i.e., number of SP  $e^-$  states and SP  $h^+$  states is equal. (f) Polarizabilities (full circles) of the Coulomb integrals  $J_{eh}$  (red),  $J_{hh}$  (green),  $J_{eh} - J_{hh}$  (purple), and of  $E_b$  computed by CI with  $12 \times 12$  SP basis (blue).

ting by Eq. (1). However, we obtained different values ranging from  $-0.5$  nm to  $0.5$  nm, depending on the  $F_d$ -range where the fit was performed. [66] We deem the aforementioned way to obtain the value of  $p_z/e$  from experiment unsatisfactory. Since the  $e^-/h^+$  wavefunctions actually experience gradually changed confinements when moving along  $z$ -axis, due to the shape of QD, the evolution of energy of QD multi-particle complexes *does not faithfully follow* equation (1).

Rather, to access  $p_z/e$  of GaAs QDs from theory, we can use directly the SP  $h^+$  and  $e^-$  states, similarly as in Refs. 19 and 53. However, this approach is reasonable only when the  $e^-/h^+$  distance is evaluated between SP ground states of those quasiparticles, available only for  $X^0$  (not  $X^+$  or any complex consisting of more than two particles) and for systems that can be reasonably well described by the SP picture, which is not the case for GaAs/AlGaAs QDs where already  $X^0$  is sizeably influ-

enced by correlation. [42]

Hence, we rather develop a method of obtaining  $\mathbf{p}/e$  directly from our CI calculations [49] as

$$\frac{\mathbf{p}}{e} = \sum_{m=1}^{n_{\text{SD}}} |\eta_m^l|^2 \left( \sum_k \frac{\langle \Psi_{h_k} | \hat{\mathbf{r}}_h | \Psi_{h_k} \rangle}{\langle \Psi_{h_k} | \Psi_{h_k} \rangle} - \sum_j \frac{\langle \Psi_{e_j} | \hat{\mathbf{r}}_e | \Psi_{e_j} \rangle}{\langle \Psi_{e_j} | \Psi_{e_j} \rangle} \right), \quad (2)$$

where  $\eta_m^l$  is the  $m$ -th element of the  $l$ -th CI matrix eigenvector  $|M^l\rangle = (\eta_1^l, \dots, \eta_{n_{\text{SD}}}^l)^T$  corresponding to  $m$ -th Slater determinant ( $\text{SD}_m$ ). Furthermore,  $\hat{\mathbf{r}}_h$  ( $\hat{\mathbf{r}}_e$ ) marks the position operator of  $h^+$  ( $e^-$ ) SP eigenstate  $|\Psi_{h_k}\rangle$  ( $|\Psi_{e_j}\rangle$ ), the indices  $j$  and  $k$  mark all SP states included in  $\text{SD}_m$ , and the bra-ket integrals are evaluated over the whole simulation space. Note, that in Eq. (2) the CI eigenstates are used as “weights” of the expectation values computed from SP states. Thus, it provides a rather general way of including the effect of correlation to the “classical” properties related to SP states.

We show the  $p_z/e$  component of Eq. (2) in Fig. 2 (a) for  $X^0$  and  $X^+$ . The calculations indicate that  $p_z/e$  of excitons confined in GaAs QDs is very small. This is very different from the situation typically encountered in strained QDs, where the dipole is mostly determined by opposite effects, the alloy gradient and the strain inhomogeneities combined with piezoelectricity. [19, 61, 67–73] Since we find that  $|p_z/e|$  is in atomic scale in both experiment and theory it is reasonable to discard  $p_z/e$  term in fitting using Eq. (1) in case of our data. [63]

In contrast to  $p_z/e$ , we find for  $\beta/e$  of  $X^0$  ( $X^+$ ) a more consistent agreement of fits by Eq. (1) between theory and experiment, see Fig. 2 (b). [66] Moreover,  $\beta/e$  shows a clear dependence on  $E_0$ . The larger QDs, with smaller  $E_0$ , tend to have larger magnitude of  $\beta_{X^0}$  ( $\beta_{X^+}$ ) for  $X^0$  ( $X^+$ ), consistent with the results reported in Ref. 65. The theoretical prediction in Refs. 39 and 68 also pointed out that with a fixed shape and chemical composition profile,  $\beta$  is mostly sensitive to the QD height. The taller QD provides in fact more room along  $z$ -direction for the confined  $e^-/h^+$  pairs to move away from each other when pulled apart by  $F_d$ , resulting in a stronger red-shift in spite of the reduced  $e^-/h^+$  binding energy.

To describe the evolution of the relative binding energy  $E_b = E(X^0) - E(X^+)$  with  $F_d$  we assume a quadratic dependence as in Eq. (1) with omitted linear term (see above discussion)

$$E_b(F_d) = E_{b,0} + \beta_{E_b}^* F_d^2, \quad (3)$$

where  $E_{b,0}$  marks  $E_b$  for  $F_d = 0$ . Thereafter, using Eq. (3) we fit the difference between  $E(X^0)$  and  $E(X^+)$  taken from corresponding dependencies in Fig. 1 (d) and we obtain the parameters  $E_{b,0}$  and  $\beta_{E_b}^*$ , which we show alongside the calculated values in Fig. 2 (c) and (d), respectively.

From Fig. 2 (c) we see that the calculated  $E_{b,0}$  is satisfyingly close to the experimental data for both the cone-

and the lens-shaped dots, in contrast to former CI calculations. [41] To the best of our knowledge, this is the first time that a positive trion binding energy as large as 5 meV is obtained from realistic calculations. The  $E_{b,0}$  values are also close to those reported in Ref. 74 ( $= E_{b,0}$  linearly increasing from  $\sim 2.4$  to  $\sim 2.9$  meV for emission energies increasing from  $\sim 1.56$  to  $\sim 1.61$  eV). We ascribe the agreement between our theory and experiment to an almost full inclusion of the correlation effects, which will be also discussed and tested in the following.

However, first let us show that the physical reason for the disagreement of Eq. (1) with theory is due to the omission of the effect of correlation as well. We start by writing the energies of the final photon states after recombination of  $X^0$  and  $X^+$  as [42, 75]  $E(X^0) = \varepsilon_e - \varepsilon_h - J_{eh,X^0} - \delta(X^0)$  and  $E(X^+) = \mathcal{E}_{X^+} - |\varepsilon_h| = \varepsilon_e - \varepsilon_h - 2J_{eh,X^+} + J_{hh} - \delta(X^+)$ , respectively. Here,  $\mathcal{E}_{X^+}$  is the energy of  $X^+$  before recombination,  $J_{eh,X^0}$ ,  $J_{eh,X^+}$ ,  $J_{hh}$  the Coulomb interactions of  $e^-h^+$  pairs in  $X^0$  and  $X^+$ , and that for  $h^+h^+$  pair, respectively;  $\varepsilon_e$  ( $\varepsilon_h$ ) is the SP  $e^-$  ( $h^+$ ) energy,  $\delta(X^0)$  ( $\delta(X^+)$ ) marks the energy change due to the effect of correlation for  $X^0$  ( $X^+$ ). Consequently, the  $E_b$  can be written as

$$E_b = 2J_{eh,X^+} - J_{eh,X^0} - J_{hh} - \delta \quad (4)$$

where  $\delta = \delta(X^0) - \delta(X^+)$ . Note that we have completely neglected the exchange interaction since we found that to be  $\approx 100$  times smaller than direct Coulomb interaction in our CI calculations. In Fig. 2 (f) we plot  $E_0$ -dependence of  $\beta_{E_b}^*/e$  for  $J_{eh}$ ,  $J_{eh} - J_{hh}$ ,  $J_{hh}$ , and  $E_{b,sim}$  from simulation. Note, that  $\beta_{E_b}^*/e$  values were obtained by fit using Eq. (3) of the theory dependencies of  $J_{eh}$ ,  $J_{eh} - J_{hh}$ ,  $J_{hh}$ , and  $E_{b,sim}$  on  $F_d$  computed by CI with  $12 \times 12$  SP basis. [76] Clearly, we find that  $\beta_{E_b}^*/e$  depends on QD size. For bigger QDs (smaller  $E_0$ ), with steeper side facets and larger height,  $|\beta_{E_b}^*/e|$  of  $J_{eh}$  is more pronounced compared to that in flatter QDs. The reason is that taller QDs facilitate the  $e^- - h^+$  separation (polarization) under the influence of vertical  $F_d$ . On the other hand,  $|\beta_{E_b}^*/e|$  for  $J_{hh}$  is smaller in larger QDs. The reason is that larger QDs allow the separation between  $h^+$  to be larger, thus reducing the Coulomb repulsion. Since the value of  $|\beta_{E_b}^*/e|$  for  $J_{hh}$  is smaller than that of  $J_{eh}$  for every QD,  $\beta_{E_b}^*$  for  $E_{b,sim}$  has larger contribution of that corresponding to  $J_{eh}$ . However, we notice that  $|\beta_{E_b}^*/e|$  for  $J_{eh} - J_{hh}$  is still smaller than that of  $E_{b,sim}$  (see the corresponding curves in Fig. 2 (f)). That means, besides  $J_{eh}$  and  $J_{hh}$  there must be another important variable in Eq. (4) changing with  $F_d$ , therefore, the correlation effect  $\delta$ , must also vary with  $F_d$ .

To prove the importance of the correlation effect in our system, we calculated  $E_b$  based on the CI model for the simulation with increasing SP basis from two  $e^-$  and two  $h^+$  ( $2 \times 2$ ) states to twenty-four  $e^-$  and twenty-four  $h^+$  ( $24 \times 24$ ) states. The result is plotted in Fig 2 (e). Clearly, in the absence of correlation, i.e., using  $2 \times 2$  and

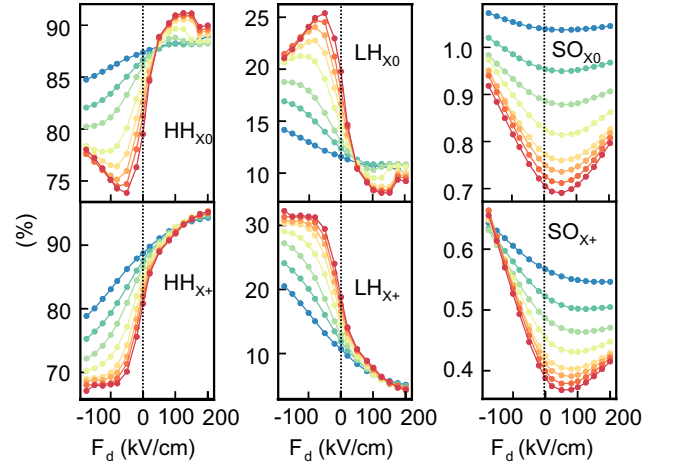


FIG. 3. Contribution of  $|HH\rangle$ ,  $|LH\rangle$  and  $|SO\rangle$  states normalized to total sum of contributions of these components, i.e.,  $z(HH) + z(LH) + z(SO)$ , in  $X^0$  (top row) and  $X^+$  (bottom row) versus electric field  $F_d$ . The colors identify the heights of QDs in the same fashion as in Fig. 2 where blue corresponds to  $h = 4$  nm and red to  $h = 9.5$  nm. The Bloch state contents for both  $X^0$  and  $X^+$  were calculated using the CI model with the basis consisting of 12 SP  $e^-$  and 12 SP  $h^+$  state, with the effects of the direct and the exchange Coulomb interaction, and the correlation effect being included.

$4 \times 4$  basis,  $X^+$  is anti-binding with respect to  $X^0$ , in contradiction with the experiment. However, with increasing basis size, the effect of correlation gains importance and  $X^+$  becomes binding with respect to  $X^0$ . The increase of  $E_b$  is steep up to  $12 \times 12$  basis, where it almost saturates. Note, that the dependence was computed for the largest considered QD, i.e.,  $h = 9.5$  nm, where the effect of correlation was expected to be the most significant.

We discuss now to the effect of  $F_d$  on heavy ( $|HH\rangle$ ), light ( $|LH\rangle$ ), and spin-orbit ( $|SO\rangle$ ) hole Bloch state mixing for  $X^0$  and  $X^+$  ground states. The corresponding normalized contents of those components, i.e.,  $z(HH) + z(LH) + z(SO)$  where  $z$  marks the respective content, is shown in Fig. 3. Note that the method of extracting the Bloch state content of CI states we developed in Ref. 42.

We observe asymmetric dependencies around  $F_d = 0$ . The content of  $|HH\rangle$  increases with  $F_d$  with a concomitant decrease in the contribution of  $|LH\rangle$  states. Since the holes are pushed towards the bottom of QD by positive  $F_d$  (Fig. 1 (c)), the  $h^+$  SP state feels little the broken translation symmetry along  $z$ -axis, since the lateral confinement is weaker at the bottom of the QD. Without broken symmetry the hole states tend not to mix, which causes an increase of the amount of  $|HH\rangle$  Bloch states. On the other hand, negative  $F_d$  ( $F_d$  applied along the opposite direction) pushes the holes towards the top of QD, thus, increasing the valence-band mixing (increase of the content of  $|LH\rangle$  and  $|SO\rangle$  Bloch states). While  $|HH\rangle$  Bloch states are purely  $|p_x\rangle$  and  $|p_y\rangle$ -like,  $|LH\rangle$  and  $|SO\rangle$

consist also of non-negligible amount of  $|p_z\rangle$  states. [77] However, for the  $|\text{SO}\rangle$  states, the same amount of  $|p_x\rangle$ ,  $|p_y\rangle$ , and  $|p_z\rangle$  Bloch states are involved, which leads to more symmetric trend than in the case of  $|\text{HH}\rangle$  and  $|\text{LH}\rangle$  states.

Now we focus on the dot size dependence of the contents of  $|\text{HH}\rangle$  and  $|\text{LH}\rangle$  Bloch states. For  $F_d < 50$  kV/cm ( $F_d < 125$  kV/cm) for  $X^0$  ( $X^+$ ), the amount of  $|\text{HH}\rangle$  ( $|\text{LH}\rangle$ ) Bloch states decreases (increases) with increasing height of the dot, as smaller QDs display larger energy separation between confined  $|\text{HH}\rangle$  and  $|\text{LH}\rangle$  SP states. Since the variation of valence band mixing is observed more pronounced in larger QDs (increased height), we observe the crossing of the HH curves for  $F_d = 50$  kV/cm ( $F_d = 125$  kV/cm) in case of  $X^0$  ( $X^+$ ). Thereafter, for  $F_d > 50$  kV/cm ( $F_d > 125$  kV/cm) for  $X^0$  ( $X^+$ ), the trend of the size dependence is reversed, i.e., bigger QDs have larger amount of  $|\text{HH}\rangle$  states than QDs with smaller height. For such large fields the dominant part of the SP hole wavefunction leaks into the wetting layer and laterally delocalizes, leading to the faster increase of the content of  $|\text{HH}\rangle$  states. We assume that for the same  $F_d$  ( $F_d > 50$  kV/cm for  $X^0$ ) all wavefunctions leak into the wetting layer with the same amount of probability density. Hence, the wavefunctions, with larger volume, i.e., for bigger QDs, consist of more  $|p_x\rangle$  and  $|p_y\rangle$  Bloch states, hence, the larger contribution of  $|\text{HH}\rangle$ .

In summary, by conducting detailed  $\mu$ -PL spectroscopy measurements of the emission from LDE-grown GaAs/AlGaAs QDs modulated by an externally applied electric field and in conjunction with conscientious calculations of multiparticle states, we reveal the influence of the electric field on the Coulomb interaction among charge carriers in GaAs QD. The experimental data and the configuration interaction calculation clearly show the dot size dependence of the polarizability of  $X^0$  and  $X^+$ . Thorough analysis of configuration interaction calculations sheds light on the deficiencies of the commonly used analysis of the quantum confined Stark effect by highlighting the striking effect of correlation and the direct Coulomb interaction energy between holes, which change with applied field and which are also significantly influenced by the asymmetry of QD along the field direction, especially in large quantum dots. Moreover, we analysed the Bloch state composition of exciton and trion complexes as a function of applied electric field and emphasize the influence of QD height as well. Finally, we note that our multiparticle simulation model based on the full configuration interaction approach with large number of single-particle basis states provides excellent quantitative agreement with the experiment, and proves the non-negligible role of correlation effect on Stark shift for the nanosystems.

The authors thank A. Haliovic, U. Kainz, J. Martín-Sánchez, T. Lettner for helpful discussions on the device fabrication. This project has received funding from

the Austrian Science Fund (FWF): FG 5, P 29603, P 30459, I 4380, I 4320, and I 3762, the Linz Institute of Technology (LIT) and the LIT Secure and Correct Systems Lab funded by the state of Upper Austria and the European Union's Horizon 2020 research and innovation program under Grant Agreement Nos. 899814 (Qurope), 654384 (ASCENT+), YH Huo is supported by NSFC (Grant No. 11774326), National Key R&D Program of China (Grant No. 2017YFA0304301) and Shanghai Municipal Science and Technology Major Project (Grant No.2019SHZDZX01). R. Trotta is supported by the European Research council (ERC) under the European Union's Horizon 2020 Research and Innovation Programme (SPQRel, Grant agreement No. 679183). D.C. and P.K. were financed by the project CUSPIDOR has received funding from the QuantERA ERA-NET Co-fund in Quantum Technologies implemented within the European Union's Horizon 2020 Programme. In addition, this project has received national funding from the Ministry of Education, Youth and Sports of the Czech Republic and funding from European Union's Horizon 2020 (2014-2020) research and innovation framework programme under grant agreement No 731473. This project 17FUN06 SIQUST has received funding from the EM-PIR programme co-financed by the Participating States and from the European Union's Horizon 2020 research and innovation programme.

---

\* huiying.emma.huang@gmail.com

† klenovskyy@physics.muni.cz

- [1] I. Aharonovich, D. Englund, and M. Toth, Solid-state single-photon emitters, *Nature Photonics* **10**, 631 (2016).
- [2] P. Senellart, G. Solomon, and A. White, High-performance semiconductor quantum-dot single-photon sources, *Nature nanotechnology* **12**, 1026 (2017).
- [3] S. Thomas and P. Senellart, The race for the ideal single-photon source is on, *Nature Nanotechnology* **16**, 367 (2021).
- [4] N. Tomm, A. Javadi, N. O. Antoniadis, D. Najer, M. C. Löbl, A. R. Korsch, R. Schott, S. R. Valentin, A. D. Wieck, A. Ludwig, and R. J. Warburton, A bright and fast source of coherent single photons, *Nature Nanotechnology* **16**, 399 (2021).
- [5] A. Orieux, M. A. Versteegh, K. D. Jöns, and S. Ducci, Semiconductor devices for entangled photon pair generation: a review, *Reports on Progress in Physics* **80**, 076001 (2017).
- [6] D. Huber, M. Reindl, J. Aberl, A. Rastelli, and R. Trotta, Semiconductor quantum dots as an ideal source of polarization-entangled photon pairs on-demand: A review, *Journal of Optics (United Kingdom)* **20**, 73002 (2018).
- [7] P. Klenovský, V. Krápek, D. Munzar, and J. Humlíček, Modelling of electronic states in InAs/GaAs quantum dots with GaAsSb strain reducing overlayer, *J. Phys.: Conf. Series* **245**, 012086 (2010).
- [8] P. Klenovský, D. Hemzal, P. Steindl, M. Zíková,



- V. Krápek, and J. Humlíček, Polarization anisotropy of the emission from type-II quantum dots, *Physical Review B* **92**, 241302(R) (2015).
- [9] E. M. Sala, I. F. Arikian, L. Bonato, F. Bertram, P. Veit, J. Christen, A. Strittmatter, and D. Bimberg, Mismatched growth of InGaAs/AlP/GAP(001) quantum dots for nanoscale memory applications, *Phys. Status Solidi B* **49**, 1800182 (2018).
- [10] M. Atatüre, D. Englund, N. Vamivakas, S. Y. Lee, and J. Wrachtrup, Material platforms for spin-based photonic quantum technologies, *Nature Reviews Materials* **3**, 38 (2018).
- [11] P. Borri, W. Langbein, S. Schneider, U. Woggon, R. L. Sellin, D. Ouyang, and D. Bimberg, Ultralong dephasing time in InGaAs quantum dots, *Physical Review Letters* **87**, 157401 (2001).
- [12] D. A. Gangloff, G. Éthier-Majcher, C. Lang, E. V. Denning, J. H. Bodey, D. M. Jackson, E. Clarke, M. Hugues, C. Le Gall, and M. Atatüre, Quantum interface of an electron and a nuclear ensemble, *Science* **364**, 62 (2019).
- [13] E. A. Chekhovich, S. F. C. da Silva, and A. Rastelli, Nuclear spin quantum register in an optically active semiconductor quantum dot, *Nature Nanotechnology* **15**, 999 (2020).
- [14] V. Krápek, P. Klenovský, A. Rastelli, O. G. Schmidt, and D. Munzar, Quantum entanglement in lateral GaAs/AlGaAs quantum dot molecules, *Quantum Dots 2010* **245**, 012027 (2010).
- [15] L. Zhai, M. C. Löbl, G. N. Nguyen, J. Ritzmann, A. Javadi, C. Spinnler, A. D. Wieck, A. Ludwig, and R. J. Warburton, Low-noise GaAs quantum dots for quantum photonics, *Nature Communications* **11**, 4745 (2020).
- [16] R. B. Patel, A. J. Bennett, I. Farrer, C. A. Nicoll, D. A. Ritchie, and A. J. Shields, Two-photon interference of the emission from electrically tunable remote quantum dots, *Nature Photonics* **4**, 632 (2010).
- [17] A. J. Bennett, R. B. Patel, J. Skiba-Szymanska, C. A. Nicoll, I. Farrer, D. A. Ritchie, and A. J. Shields, Giant Stark effect in the emission of single semiconductor quantum dots, *Applied Physics Letters* **97**, 031104 (2010).
- [18] R. Trotta, E. Zallo, E. Magerl, O. G. Schmidt, and A. Rastelli, Independent control of exciton and biexciton energies in single quantum dots via electroelastic fields, *Physical Review B - Condensed Matter and Materials Physics* **88**, 155312 (2013).
- [19] J. Aberl, P. Klenovský, J. S. Wildmann, J. Martin-Sanchez, T. Fromherz, E. Zallo, J. Humlíček, A. Rastelli, and R. Trotta, Inversion of the exciton built-in dipole moment in In(Ga)As quantum dots via nonlinear piezoelectric effect, *Physical Review B* **96**, 045414 (2017).
- [20] M. Gurioli, Z. Wang, A. Rastelli, T. Kuroda, and S. Sanguinetti, Droplet epitaxy of semiconductor nanostructures for quantum photonic devices, *Nature Materials* **18**, 799 (2019).
- [21] C. Heyn, A. Stemann, T. Köppen, C. Strelow, T. Kipp, M. Grave, S. Mendach, and W. Hansen, Highly uniform and strain-free GaAs quantum dots fabricated by filling of self-assembled nanoholes, *Applied Physics Letters* **94**, 183113 (2009).
- [22] C. Heyn, M. Klingbeil, C. Strelow, A. Stemann, S. Mendach, and W. Hansen, Single-dot Spectroscopy of GaAs Quantum Dots Fabricated by Filling of Self-assembled Nanoholes, *Nanoscale Research Letters* **5**, 1633 (2010).
- [23] H. Huang, S. Manna, C. Schimpf, M. Reindl, X. Yuan, Y. Zhang, S. Filipe Covre da Silva, and A. Rastelli, Bright single photon emission from quantum dots embedded in a broadband planar optical antenna, *Advanced Optical Materials* **9**, 2001490 (2021).
- [24] C. Heyn, A. Stemann, T. Köppen, C. Strelow, T. Kipp, M. Grave, S. Mendach, and W. Hansen, Optical properties of GaAs quantum dots fabricated by filling of self-assembled nanoholes, *Nanoscale Research Letters* **5**, 576 (2010).
- [25] Y. H. Huo, A. Rastelli, and O. G. Schmidt, Ultra-small excitonic fine structure splitting in highly symmetric quantum dots on GaAs (001) substrate, *Applied Physics Letters* **102**, 152105 (2013).
- [26] C. Heyn, S. Schnüll, and W. Hansen, Scaling of the structural characteristics of nanoholes created by local droplet etching, *Journal of Applied Physics* **115**, 024309 (2014).
- [27] E. Schöll, L. Hanschke, L. Schweickert, K. D. Zeuner, M. Reindl, S. F. Covre Da Silva, T. Lettner, R. Trotta, J. J. Finley, K. Müller, A. Rastelli, V. Zwiller, and K. D. Jöns, Resonance Fluorescence of GaAs Quantum Dots with Near-Unity Photon Indistinguishability, *Nano Letters* **19**, 2404 (2019).
- [28] D. Huber, M. Reindl, S. F. Covre da Silva, C. Schimpf, J. Martin-Sanchez, H. Huang, G. Piredda, J. Edlinger, A. Rastelli, and R. Trotta, Strain-Tunable GaAs Quantum Dot: A Nearly Dephasing-Free Source of Entangled Photon Pairs on Demand, *Physical Review Letters* **121**, 033902 (2018).
- [29] M. Zopf, R. Keil, Y. Chen, J. Yang, D. Chen, F. Ding, and O. G. Schmidt, Entanglement Swapping with Semiconductor-Generated Photons Violates Bell's Inequality, *Physical Review Letters* **123**, 160502 (2019).
- [30] F. Basso Basset, M. B. Rota, C. Schimpf, D. Tedeschi, K. D. Zeuner, S. F. Covre da Silva, M. Reindl, V. Zwiller, K. D. Jöns, A. Rastelli, and R. Trotta, Entanglement Swapping with Photons Generated on Demand by a Quantum Dot, *Physical Review Letters* **123**, 160501 (2019).
- [31] F. Basso Basset, M. Valeri, E. Roccia, V. Muredda, D. Poderini, J. Neuwirth, N. Spagnolo, M. B. Rota, G. Carvacho, F. Sciarrino, and R. Trotta, Quantum key distribution with entangled photons generated on demand by a quantum dot, *Science advances* **7**, 1 (2021).
- [32] C. Schimpf, M. Reindl, D. Huber, B. Lehner, S. F. Covre Da Silva, S. Manna, M. Vyvlecka, P. Walther, and A. Rastelli, Quantum cryptography with highly entangled photons from semiconductor quantum dots, *Science Advances* **7**, abe8905 (2021).
- [33] R. Singh, Tuning fine structure splitting and exciton emission energy in semiconductor quantum dots, *Journal of Luminescence* **202**, 118 (2018).
- [34] M. V. Durnev, M. Vidal, L. Bouet, T. Amand, M. M. Glazov, E. L. Ivchenko, P. Zhou, G. Wang, T. Mano, N. Ha, T. Kuroda, X. Marie, K. Sakoda, and B. Urbaszek, Magnetospectroscopy of excited states in charge-tunable GaAs/AlGaAs [111] quantum dots, *Physical Review B* **93**, 245412 (2016).
- [35] N. Ha, T. Mano, Y.-L. Chou, Y.-N. Wu, S.-J. Cheng, J. Bocquel, P. M. Koenraad, A. Ohtake, Y. Sakuma, K. Sakoda, and T. Kuroda, Size-dependent line broadening in the emission spectra of single GaAs quantum dots: Impact of surface charge on spectral diffusion, *Phys. Rev.*

- B **92**, 075306 (2015).
- [36] F. Langer, D. Plischke, M. Kamp, and S. Höfling, Single photon emission of a charge-tunable GaAs/Al 0.25 Ga 0.75 As droplet quantum dot device, *Applied Physics Letters* **105**, 081111 (2014).
- [37] S. Marcet, K. Ohtani, and H. Ohno, Vertical electric field tuning of the exciton fine structure splitting and photon correlation measurements of GaAs quantum dot, *Applied Physics Letters* **96**, 101117 (2010).
- [38] M. Ghali, K. Ohtani, Y. Ohno, and H. Ohno, Generation and control of polarization-entangled photons from GaAs island quantum dots by an electric field, *Nature Communications* **3**, 1 (2012).
- [39] C. Heyn, L. Ransinghe, M. Zocher, and W. Hansen, Shape-Dependent Stark Shift and Emission-Line Broadening of Quantum Dots and Rings, *Journal of Physical Chemistry C* **124**, 19809 (2020).
- [40] A. Rastelli, S. Stufler, A. Schliwa, R. Songmuang, C. Manzano, G. Costantini, K. Kern, A. Zrenner, D. Bimberg, and O. G. Schmidt, Hierarchical self-assembly of GaAs/AlGaAs quantum dots, *Physical Review Letters* **92**, 166104 (2004).
- [41] L. Wang, V. Krápek, F. Ding, F. Horton, A. Schliwa, D. Bimberg, A. Rastelli, and O. G. Schmidt, Self-assembled quantum dots with tunable thickness of the wetting layer: Role of vertical confinement on interlevel spacing, *Physical Review B - Condensed Matter and Materials Physics* **80**, 085309 (2009).
- [42] D. Csontosová and P. Klenovský, Theory of magneto-optical properties of neutral and charged excitons in GaAs/AlGaAs quantum dots, *Physical Review B* **102**, 125412 (2020).
- [43] Z. Trabelsi, M. Yahyaoui, K. Boujdaria, M. Chamarro, and C. Testelin, Excitonic complexes in strain-free and highly symmetric GaAs quantum dots fabricated by filling of self-assembled nanoholes, *Journal of Applied Physics* **121**, 245702 (2017).
- [44] A. Graf, D. Sonnenberg, V. Paulava, A. Schliwa, C. Heyn, and W. Hansen, Excitonic states in GaAs quantum dots fabricated by local droplet etching, *Physical Review B - Condensed Matter and Materials Physics* **89**, 115314 (2014).
- [45] P. Atkinson, E. Zallo, and O. Schmidt, Independent wavelength and density control of uniform gaas/algaas quantum dots grown by infilling self-assembled nanoholes, *Journal of Applied Physics* **112**, 054303 (2012).
- [46] D. Huber, B. U. Lehner, D. Csontosová, M. Reindl, S. Schuler, S. F. Covre da Silva, P. Klenovský, and A. Rastelli, Single-particle-picture breakdown in laterally weakly confining GaAs quantum dots, *PHYSICAL REVIEW B* **100**, 235425 (2019).
- [47] J. Shumway, A. Franceschetti, and A. Zunger, Correlation versus mean-field contributions to excitons, multiexcitons, and charging energies in semiconductor quantum dots, *Physical Review B - Condensed Matter and Materials Physics* **63**, 155316 (2001).
- [48] A. Schliwa, M. Winkelnkemper, and D. Bimberg, Few-particle energies versus geometry and composition of In<sub>x</sub>Ga<sub>1-x</sub>As/GaAs self-organized quantum dots, *Physical Review B - Condensed Matter and Materials Physics* **79**, 075443 (2009).
- [49] P. Klenovský, P. Steindl, and D. Geffroy, Excitonic structure and pumping power dependent emission blue-shift of type-II quantum dots, *Scientific Reports* **7**, 45568 (2017).
- [50] P. Klenovský, A. Schliwa, and D. Bimberg, Electronic states of (inga)(assb)/gaas/gap quantum dots, *Phys. Rev. B* **100**, 115424 (2019).
- [51] G. Bester, A. Zunger, X. Wu, and D. Vanderbilt, Effects of linear and nonlinear piezoelectricity on the electronic properties of InAsGaAs quantum dots, *Physical Review B - Condensed Matter and Materials Physics* **74**, 081305(R) (2006).
- [52] A. Beya-Wakata, P.-Y. Prodhomme, and G. Bester, First- and second-order piezoelectricity in III-V semiconductors, *Phys. Rev. B* **84**, 195207 (2011).
- [53] P. Klenovský, P. Steindl, J. Aberl, E. Zallo, R. Trotta, A. Rastelli, and T. Fromherz, Effect of second-order piezoelectricity on the excitonic structure of stress-tuned In(Ga)As/GaAs quantum dots, *Physical Review B* **97**, 245314 (2018).
- [54] S. Birner, T. Zibold, T. Andlauer, T. Kubis, M. Sabathil, A. Trellakis, and P. Vogl, Nextnano: General purpose 3-D simulations, *IEEE Transactions on Electron Devices* **54**, 2137 (2007).
- [55] Y. H. Huo, V. Krápek, A. Rastelli, and O. G. Schmidt, Volume dependence of excitonic fine structure splitting in geometrically similar quantum dots, *Physical Review B - Condensed Matter and Materials Physics* **90**, 041304(R) (2014).
- [56] See Supplemental Material at [URL will be inserted by publisher] for section SI. describing the details on the QD and LED growth. ().
- [57] Y. Arashida, Y. Ogawa, and F. Minami, Correlated photons from multi-carrier complexes in GaAs quantum dots, *Superlattices and Microstructures* **47**, 93 (2010).
- [58] D. V. Regelman, E. Dekel, D. Gershoni, E. Ehrenfreund, A. J. Williamson, J. Shumway, A. Zunger, W. V. Schoenfeld, and P. M. Petroff, Optical spectroscopy of single quantum dots at tunable positive, neutral, and negative charge states, *Physical Review B - Condensed Matter and Materials Physics* **64**, 165301 (2001).
- [59] J. J. Finley, M. Sabathil, P. Vogl, G. Abstreiter, R. Oulton, A. I. Tartakovskii, D. J. Mowbray, M. S. Skolnick, S. L. Liew, A. G. Cullis, and M. Hopkinson, Quantum-confined Stark shifts of charged exciton complexes in quantum dots, *Physical Review B - Condensed Matter and Materials Physics* **70**, 201308(R) (2004).
- [60] H. Huang, R. Trotta, Y. Huo, T. Lettner, J. S. Wildmann, J. Martín-Sánchez, D. Huber, M. Reindl, J. Zhang, E. Zallo, O. G. Schmidt, and A. Rastelli, Electrically-Pumped Wavelength-Tunable GaAs Quantum Dots Interfaced with Rubidium Atoms, *ACS Photonics* **4**, 868 (2017).
- [61] P. Jin, C. M. Li, Z. Y. Zhang, F. Q. Liu, Y. H. Chen, X. L. Ye, B. Xu, and Z. G. Wang, Quantum-confined Stark effect and built-in dipole moment in self-assembled InAs/GaAs quantum dots, *Applied Physics Letters* **85**, 2791 (2004).
- [62] J. D. Mar, J. J. Baumberg, X. L. Xu, A. C. Irvine, and D. A. Williams, Precise measurements of the dipole moment and polarizability of the neutral exciton and positive trion in a single quantum dot, *Physical Review B* **95**, 201304(R) (2017).
- [63] See Supplemental Material at [URL will be inserted by publisher] for section SII. giving the fits by Eq. (1) with and without considering the linear term. ().
- [64] See Supplemental Material at [URL will be inserted by

- publisher] for section SIII. giving the values of the fitted  $p_z/e$  and  $\beta$  of five studied dots. ().
- [65] M. Ghali, Y. Ohno, and H. Ohno, Vertical electric field induced suppression of fine structure splitting of excited state excitons in a single GaAs/AlGaAs island quantum dots, *Applied Physics Letters* **107**, 123102 (2015).
- [66] See Supplemental Material at [URL will be inserted by publisher] for section SIV. for the fits of theory data by Eq. (1) performed in different intervals of  $F_d$ . ().
- [67] M. Grundmann, O. Stier, and D. Bimberg, Inas/gaas pyramidal quantum dots - strain distribution, optical phonons, and electronic-structure, *Physical Review B* **52**, 11969 (1995).
- [68] J. A. Barker and E. P. O'Reilly, Theoretical analysis of electron-hole alignment in inas-gaas quantum dots, *Physical Review B* **61**, 13840 (2000).
- [69] P. W. Fry, I. E. Itskevich, D. J. Mowbray, M. S. Skolnick, J. J. Finley, J. A. Barker, E. P. O'Reilly, L. R. Wilson, I. A. Larkin, P. A. Maksym, M. Hopkinson, M. Al-Khafaji, J. P. R. David, A. G. Cullis, G. Hill, and J. C. Clark, Inverted electron-hole alignment in inas-gaas self-assembled quantum dots, *Physical Review Letters* **84**, 733 (2000).
- [70] K. Chang and J. B. Xia, Asymmetric stark shifts of exciton in inas/gaas pyramidal quantum dots, *Solid State Communications* **104**, 351 (1997).
- [71] F. Findeis, M. Baier, E. Beham, A. Zrenner, and G. Abstreiter, Photocurrent and photoluminescence of a single self-assembled quantum dot in electric fields, *Applied Physics Letters* **78**, 2958 (2001).
- [72] T. M. Hsu, W. H. Chang, C. C. Huang, N. T. Yeh, and J. I. Chyi, Quantum-confined stark shift in electroreflectance of inas/inxgal-xas self-assembled quantum dots, *Applied Physics Letters* **78**, 1760 (2001).
- [73] W. D. Sheng and J. P. Leburton, Enhanced intraband transitions with strong electric-field asymmetry in stacked inas/gaas self-assembled quantum dots, *Physical Review B* **64**, 153302 (2001).
- [74] M. C. Löbl, L. Zhai, J.-P. Jahn, J. Ritzmann, Y. Huo, A. D. Wieck, O. G. Schmidt, A. Ludwig, A. Rastelli, and R. J. Warburton, Correlations between optical properties and voronoi-cell area of quantum dots, *Phys. Rev. B* **100**, 155402 (2019).
- [75] A. Schliwa and M. Winkelnkemper, Theory of excitons in ingaas/gaas quantum dots, in *Semiconductor Nanostructures*, edited by D. Bimberg (Springer Berlin Heidelberg, 2008) pp. 139–164.
- [76] See Supplemental Material at [URL will be inserted by publisher] for section SV. for the dependencies of the computed direct Coulomb integrals on  $F_d$  and the corresponding fits. ().
- [77] See Supplemental Material at [URL will be inserted by publisher] for section SVI. for the equations giving the conversion between  $\{|S\rangle, |HH\rangle, |LH\rangle, |SO\rangle\} \otimes \{|\uparrow\rangle, |\downarrow\rangle\}$  Bloch states and  $\{|s\rangle, |p_x\rangle, |p_y\rangle, |p_z\rangle\} \otimes \{|\uparrow\rangle, |\downarrow\rangle\}$  Bloch states. ().